GBT MEMO 78

National Radio Astronomy Observatory
Charlottesville, Virginia 22903

CORRECTING FOR GRAVITY INDUCED DEFORMATIONS

S. Srikanth
May 20, 1992

GBT Memo #48 presents computed performance results of the GBT when the feed and subreflector travel by 8.00", relative to the main reflector, in the symmetric plane. This travel is due to the predicted deflection of the feed support arm when the telescope moves from zenith to horizon, from an analysis done on an initial NRAO structural design. The information about the deformation of the main reflector was not available then. Analytical work by C. Merrill on the NASTRAN model of Loral's preliminary design of the elevation structure has shed more light on the deformation of the structure at present. This memo analyzes the performance of the GBT, resulting from the deformation of the main reflector and the feed support arm, induced by gravity, as the telescope moves in elevation from the rigging elevation of 30°. An attempt has been made to correct for the loss in efficiency by translating the subreflector in the symmetric plane. The prime goal of this analysis is to investigate whether the gain loss due to the deformations can be recovered by subreflector translation. In the process, however, some pointing information and amounts of travel required on the subreflector actuators have become available. An assumption made here is that the main reflector deforms to some best-fit paraboloid and the active surface removes the remaining surface errors.

The analysis is carried out from the secondary focus at 1.42, 8.00, 20.00 and 50.00 GHz. At 30° elevation, the main reflector is a perfect paraboloid of 60 meter focal length and the selected feed is located at the secondary focus which is coincident with one of the focii of the ellipsoidal subreflector (Figure 1). At horizon the main reflector deforms to a paraboloid of focal length 59.884 m with its axis rotated clockwise (negative rotation in Figure 1) by 4.5 arcminutes. Table 1 gives the amount of travel of the vertex of the main reflector, the focus of the paraboloid, subreflector attachment point and the turret. The coordinates used are shown in Figure 1. At zenith the focal length of the deformed parabola is 60.120 m and the angle of rotation of its axis is 9.4 arcminutes in the counterclockwise (positive) direction. These numbers are derived from the analysis of the NASTRAN model.

TABLE 1. Δ FROM THE RIGGING POSITION

	Horizon		Zenith	
	Y (ins)	Z (ins)	Y (ins)	Z (ins)
Main reflector vertex	-1.938	1.725	4.435	-3.642
Focus	1.170	-2.842	-2.042	1.055
Subreflector	5.682	3.265	-16.353	-5.430
Feed	4.506	2.842	-12.587	-4.615

The efficiency of the telescope is calculated at 30° elevation, horizon and zenith. Table 2 lists the efficiencies at horizon before and after correction is applied, while Table 3 shows the efficiencies at zenith. The correction, as referred to here, is the compensation for the deformations. The surface rms efficiency is not included in these calculations. As seen from column 4 of Tables 2 and 3, the loss in efficiency before correction is higher for the zenith case, as compared to horizon, consistent with the larger deformations at zenith. The efficiency loss is due to a combination of increased spillover and phase error introduced in the aperture, as the feed and subreflector have moved relative to the main reflector. Figure 2 gives the far-field patterns at different frequencies in the symmetric plane at 30° elevation. Figures 3 and 4 give the far-field patterns in the symmetric and asymmetric planes at horizon at 1.42 and 20.00 GHz, respectively, before any correction is applied, while Figures 5 and 6 give the patterns at zenith. The beam axis in Figures 3a and 4a is 4.5 arcminutes (see Figure 1 for sense of rotation) from the axis of the undeformed paraboloid, while that in Figures 5a and 6a is -9.2 arcminutes from the paraboloid axis. The beam directivity is lost even at 8.00 GHz. The feed is no longer at the focus of the subreflector, and neither the feed nor the subreflector is at the optimum position with respect to the deformed parabola. The feed is fixed in space and the only correction that can be applied is through the translation of the subreflector. As a first attempt, the subreflector is moved so that one of its focii is at the phase center of the feed. The loss in efficiency at 1.42 GHz is 2.4% at horizon and 7.2% at zenith and is still very high at higher frequencies, as shown in column 6 of Tables 2 and 3.

In the second iteration, given the deformed best-fit paraboloid parameters and the subreflector parameters which have not changed, the position of the secondary focus is located for the combination of the best-fit paraboloid and the subreflector. The subreflector is now moved to this focus position. At 1.42 GHz the gain loss is fully recovered both at horizon and zenith. The efficiency loss at 50 GHz is 19.2% at horizon and as high as 69% at zenith (column 8). This can be attributed to the fact that the feed is still not at the secondary focus and also the subreflector axis is not at the appropriate angle with respect to the axis of the parabola. The fact that the loss in efficiency is higher at higher frequencies indicates that it is mainly due to the phase error in the aperture. The subreflector is then translated in two orthogonal directions to minimize the phase error. As seen from the last column of the tables, the efficiency is back to where it was at the rigging angle, at all frequencies for the zenith case. At horizon, however, the loss in efficiency is 0.55% at 20 GHz and 2.40% at 50 GHz. This may be because the optimum position for the subreflector has not been found at horizon. Figures 7 through 10 show the far-field patterns after correction at horizon and Figures 11 through 15 show patterns at zenith. The translations that are required of the subreflector are shown in Table 4.

TABLE 4. SUBREFLECTOR TRANSLATIONS

	Y (ins)	Z (ins)
Horizon	-5.05	-5.62
Zenith	14.63	6.12

The axes are as in Figure 1. These translations are referred to with respect to the deformed paraboloid axes at zenith and horizon. However, the angles of rotation of these axes with reference to the original paraboloid axis being small, the translation magnitudes for the subreflector are good to a first order. Thus, total travels of about 20.0" and 12.0" perpendicular and along the axis of the main reflector, respectively, are required for the subreflector positioner mechanism.

Finally, the pointing error at horizon is -6.8 arcminutes; at zenith, it is 14.6 arcminutes. These are the pointing errors after the subreflector has been moved to the position where all the gain loss is recovered. The conclusion of this memo is that the subreflector translations can largely compensate for the loss in efficiency caused by gravity-induced deformations, provided the active surface has been used to remove the surface rms errors. The pointing errors addressed in this memo are assumed repeatable and, if repeatable, can be corrected through the antenna az-el drives.

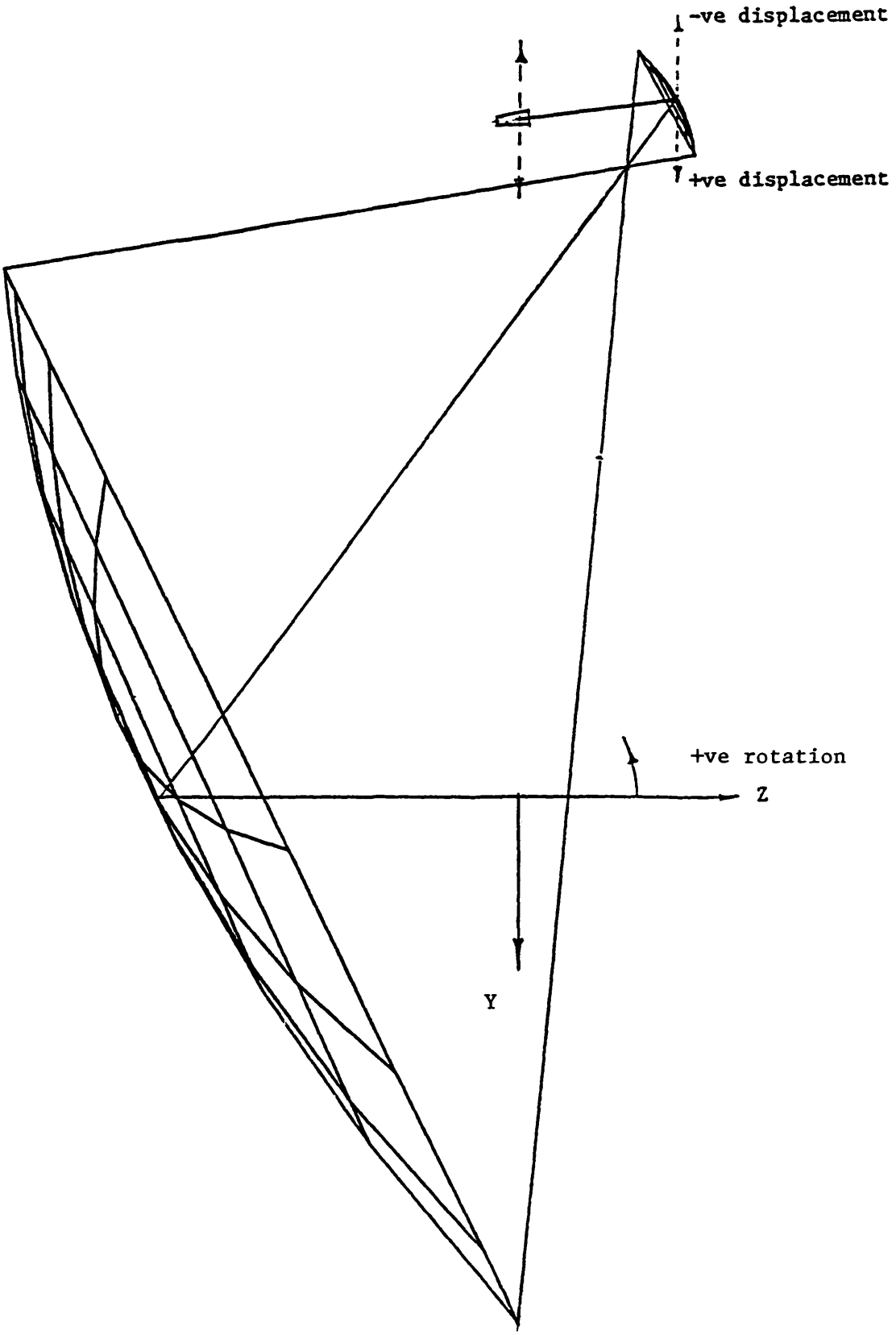

Figure 1. Geometry of the GBT

TABLE 2. APERTURE EFFICIENCY AT HORIZON

Freq. (GHz)	30° Elevation	Horizon							
		Before Correction		Subrefl. Focus at Feed Phase Center		Subrefl. at Optimum Position of Deformed Paraboloid		Subrefl. Translated for Minimum Phase Error	
	η_0 (%)	η (%)	$\frac{\eta_0 - \eta}{\eta_0}$ (%)	η (%)	$\frac{\eta_0 - \eta}{\eta_0}$ (%)	η (%)	$\frac{\eta_0 - \eta}{\eta_0}$ (%)	η (%)	$\frac{\eta_0 - \eta}{\eta_0}$ (%)
1.42	71.8201	69.8757	2.71	70.1207	2.37	71.8201	0	71.8201	0
8.00	73.5839	29.3246	60.15	33.2157	54.86	73.3555	0.31	73.5839	0
20.00	74.3144	7.3000	90.18	9.0422	87.83	71.8444	3.32	73.9031	0.55
50.00	74.5131	1.6405	97.80			60.1787	19.24	72.7248	2.40

TABLE 3. APERTURE EFFICIENCY AT ZENITH

Freq. (GHz)	30° Elevation	Zenith							
		Before Correction		Subrefl. Focus at Feed Phase Center		Subrefl. at Optimum Position of Deformed Paraboloid		Subrefl. Translated for Minimum Phase Error	
	η_0 (%)	η (%)	$\frac{\eta_0 - \eta}{\eta_0}$ (%)	η (%)	$\frac{\eta_0 - \eta}{\eta_0}$ (%)	η (%)	$\frac{\eta_0 - \eta}{\eta_0}$ (%)	η (%)	$\frac{\eta_0 - \eta}{\eta_0}$ (%)
1.42	71.8201	61.3474	14.58	66.1509	7.20	71.8201	0	71.8201	0
8.00	73.5839	14.4349	80.38	17.9446	75.61	72.0714	2.06	73.5839	0
20.00	74.3144	5.6302	92.42	6.4791	91.28	61.2608	17.56	74.3144	0
50.00	74.5131	1.4593	98.04			23.2051	68.86	74.5131	0

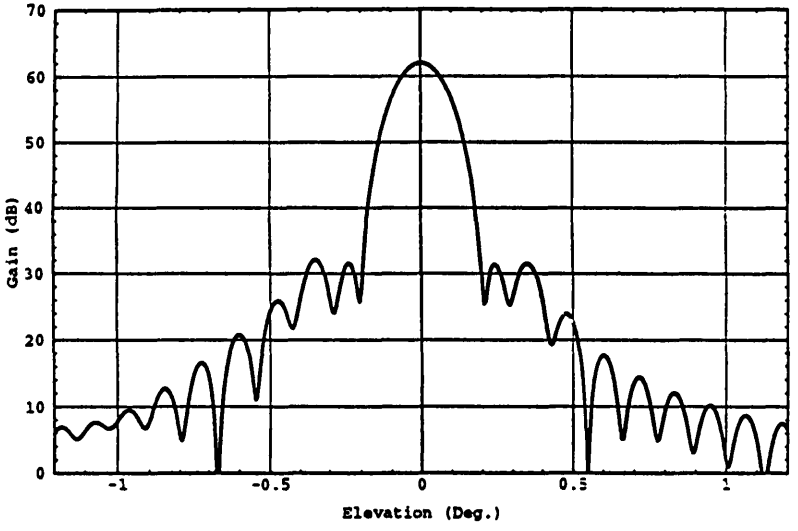

(a) 1.42 GHz

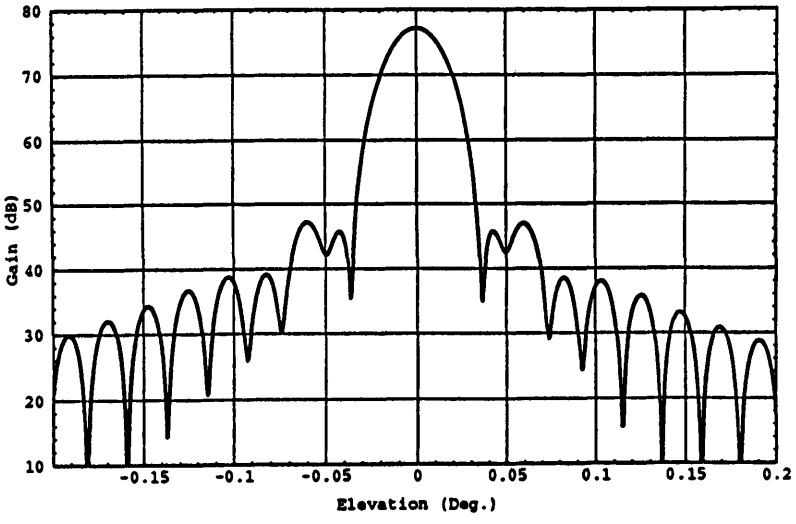

(b) 8.00 GHz

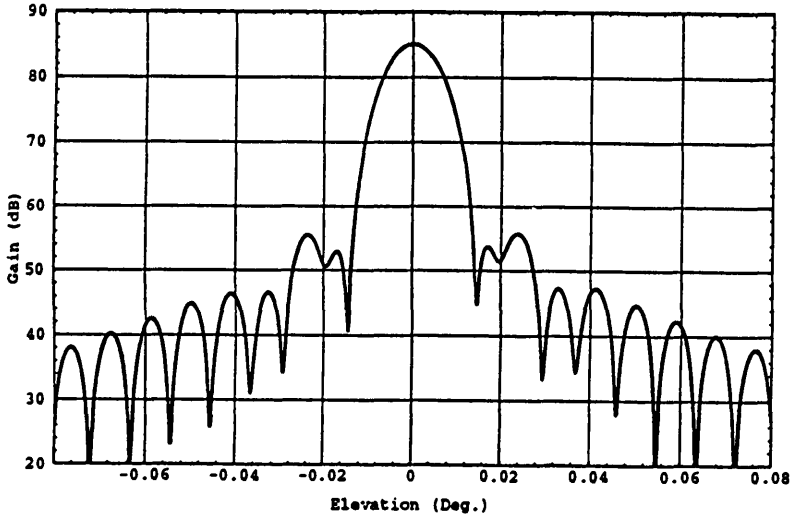

(c) 20.00 GHz

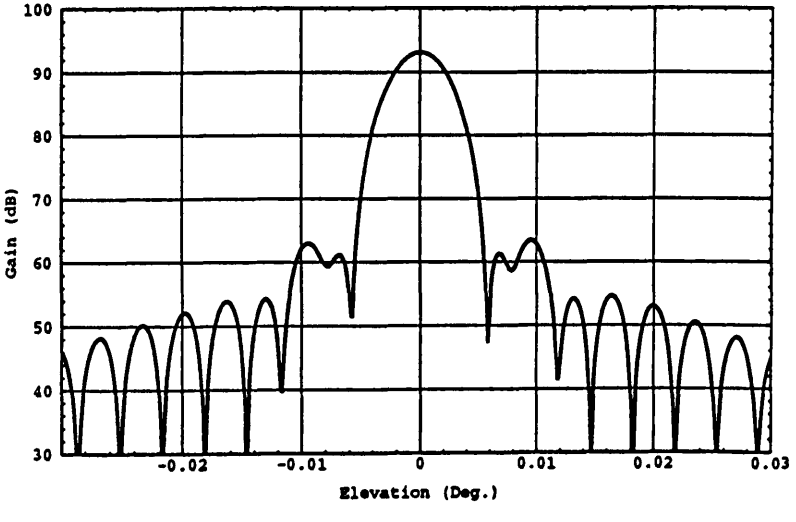

(d) 50.00 GHz

Fig. 2. Far-field pattern in symmetric plane at 30° elevation.

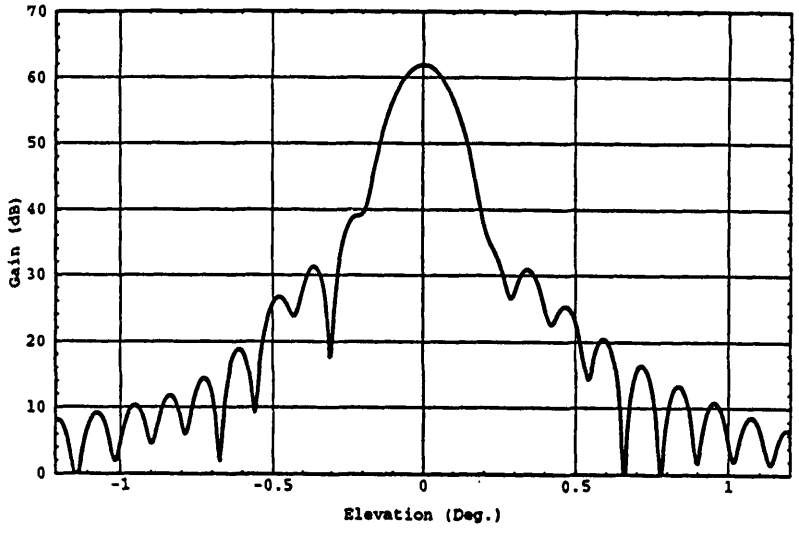

(a) Symmetric plane

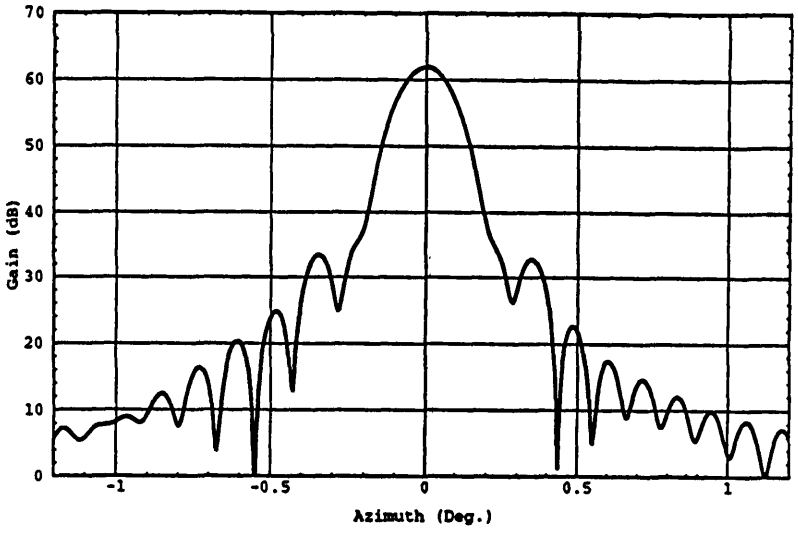

(b) Asymmetric plane

Fig. 3. Far-field pattern at 1.42 GHz at horizon before correction.

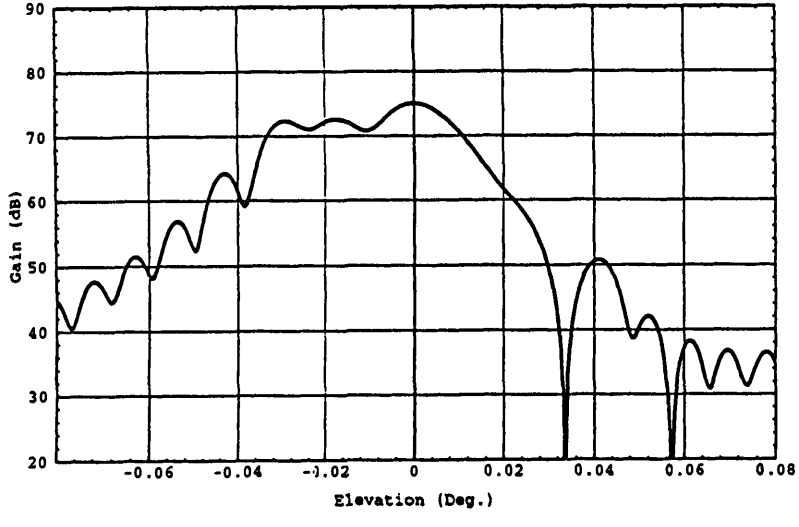

(a) Symmetric plane

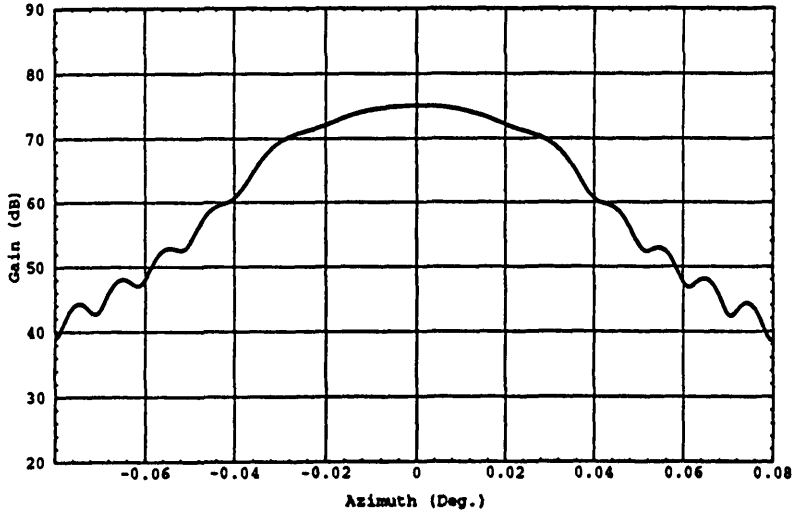

(b) Asymmetric plane

Fig. 4. Far-field pattern at 20.00 GHz at horizon before correction.

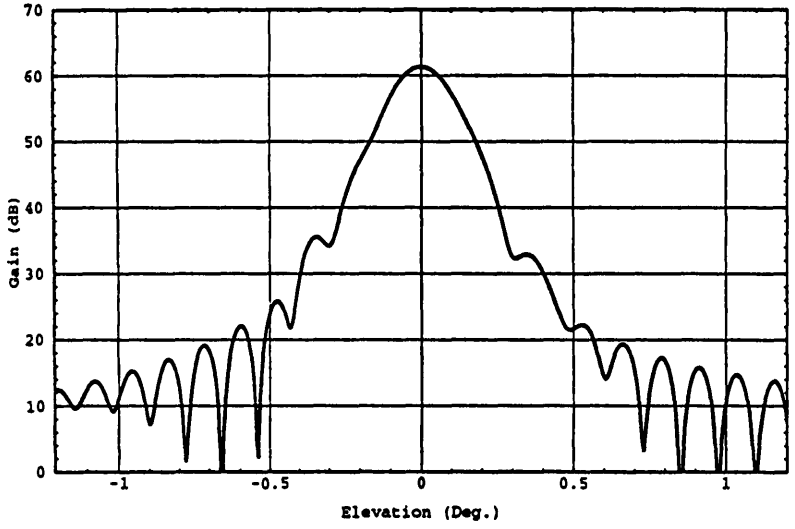

(a) Symmetric plane

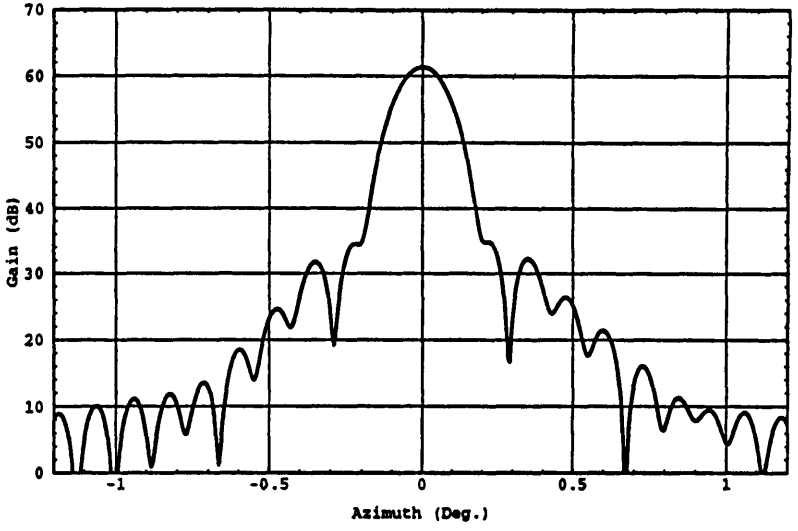

(b) Asymmetric plane

Fig. 5. Far-field pattern at 1.42 GHz at zenith before correction.

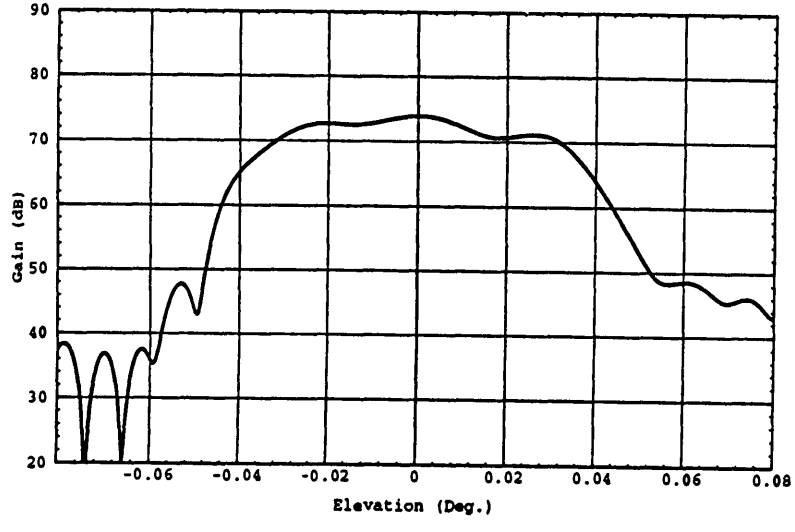

(a) Symmetric plane

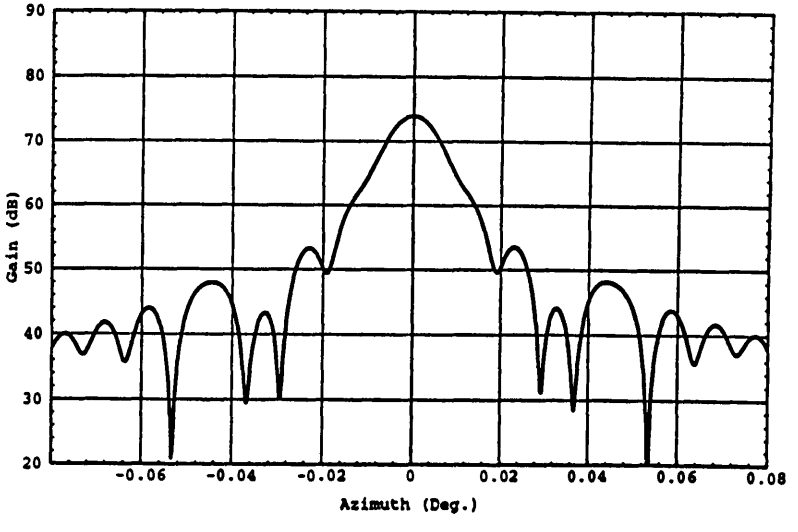

(b) Asymmetric plane

Fig. 6. Far-field pattern at 20.00 GHz at zenith before correction.

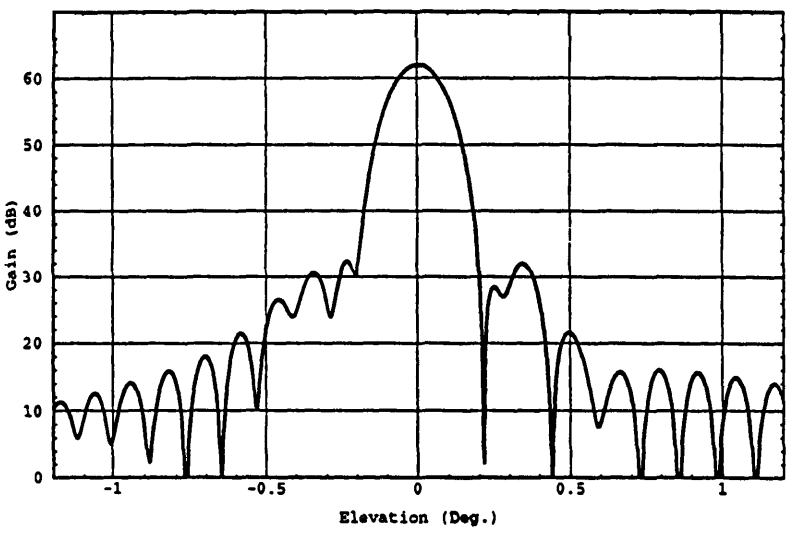

(a) Symmetric plane

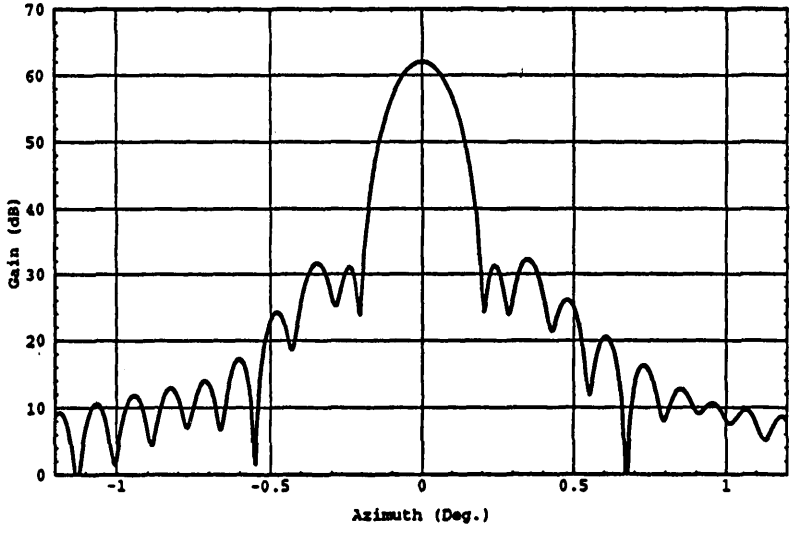

(b) Asymmetric plane

Fig. 7. Far-field pattern at 1.42 GHz at horizon after correction.

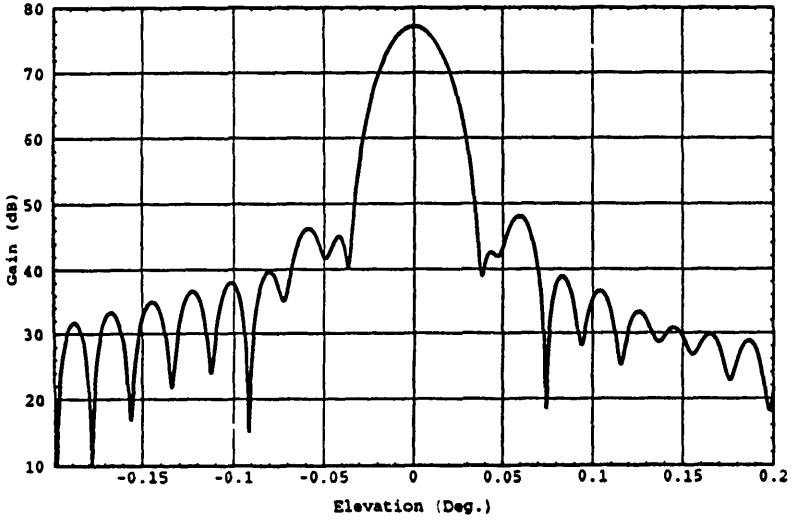

(a) Symmetric plane

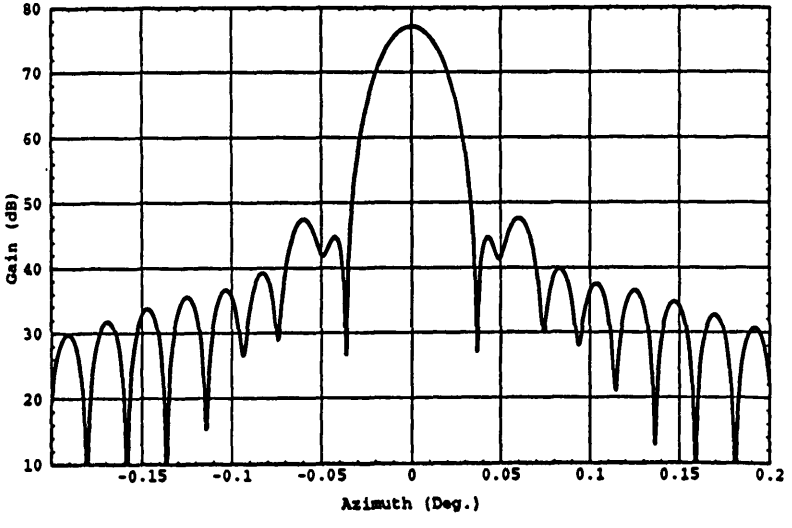

(b) Asymmetric plane

Fig. 8. Far-field pattern at 8.00 GHz at horizon after correction.

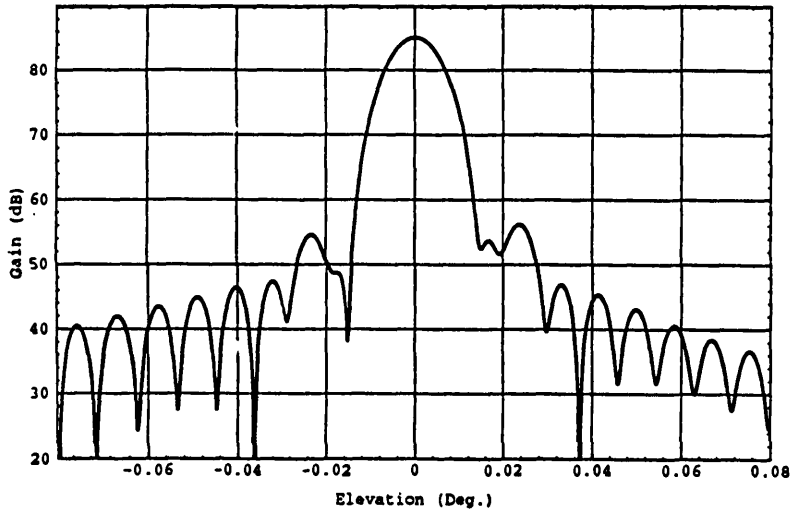

(a) Symmetric plane

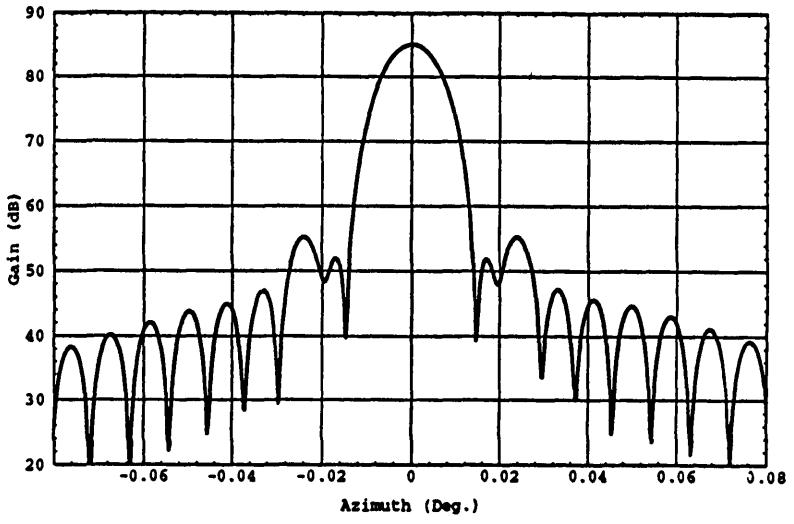

(b) Asymmetric plane

Fig. 9. Far-field pattern at 20.00 GHz at horizon after correction.

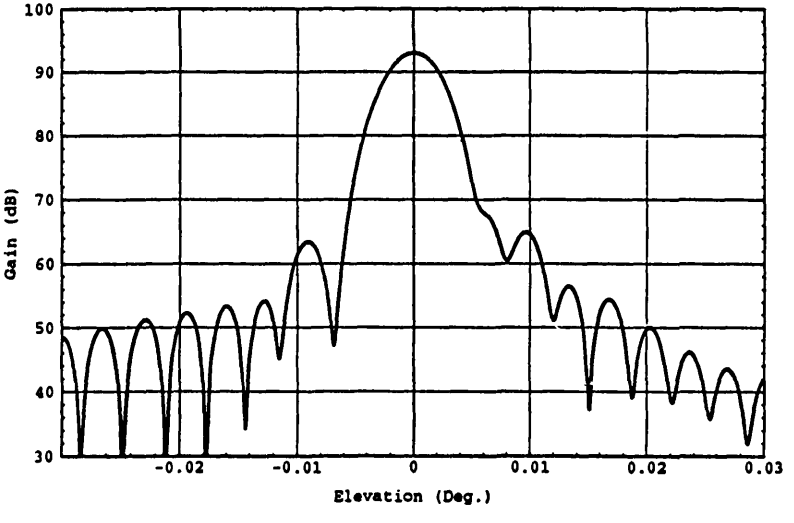

(a) Symmetric plane

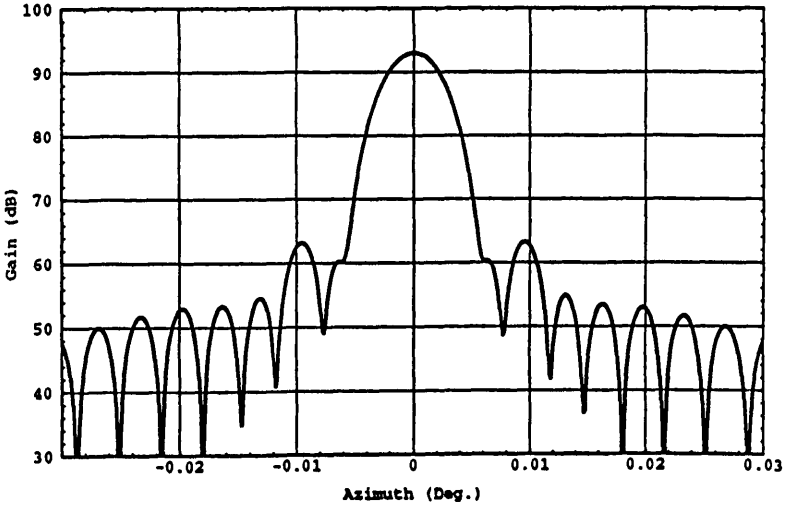

(b) Asymmetric plane

Fig. 10. Far-field pattern at 50.00 GHz at horizon after correction.

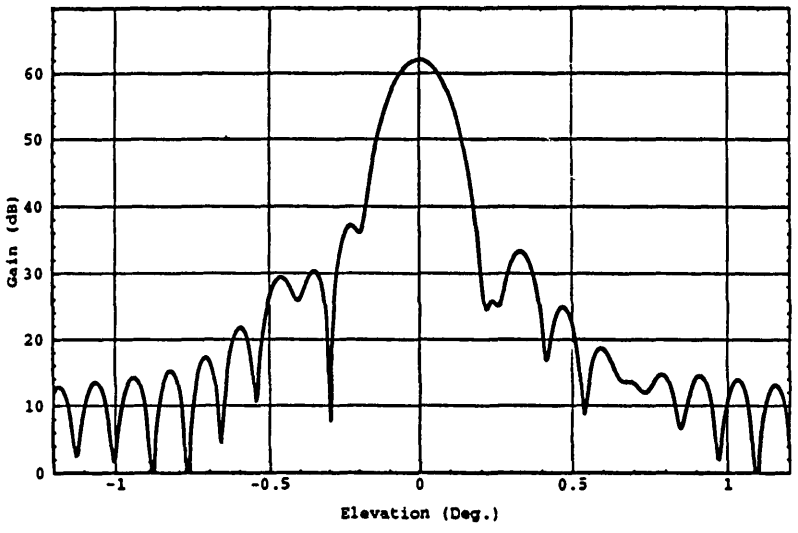

(a) Symmetric plane

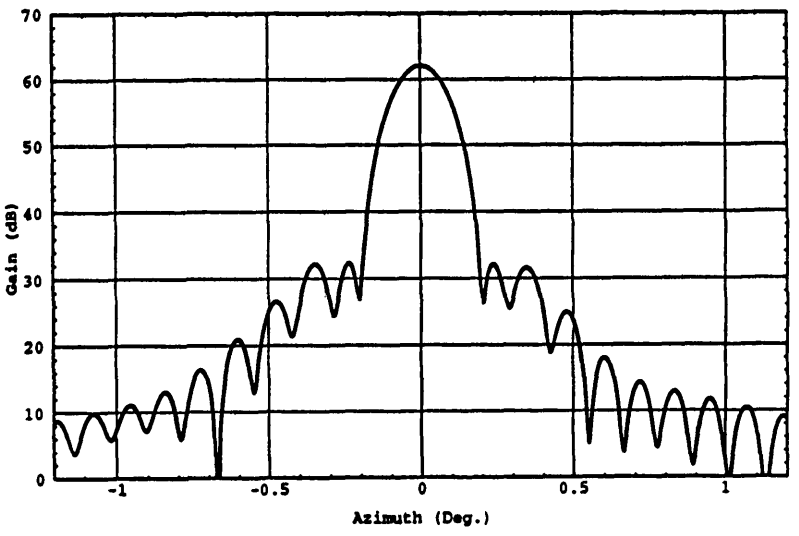

(b) Asymmetric plane

Fig. 11. Far-field pattern at 1.42 GHz at zenith after correction.

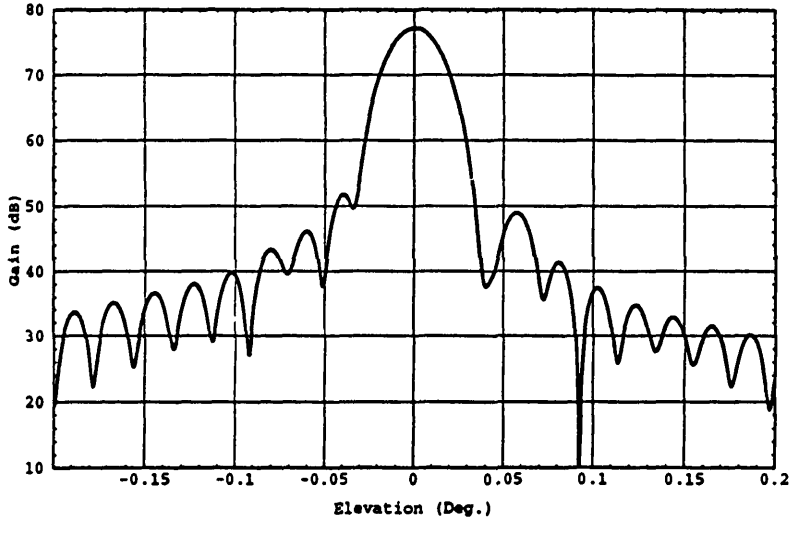

(a) Symmetric plane

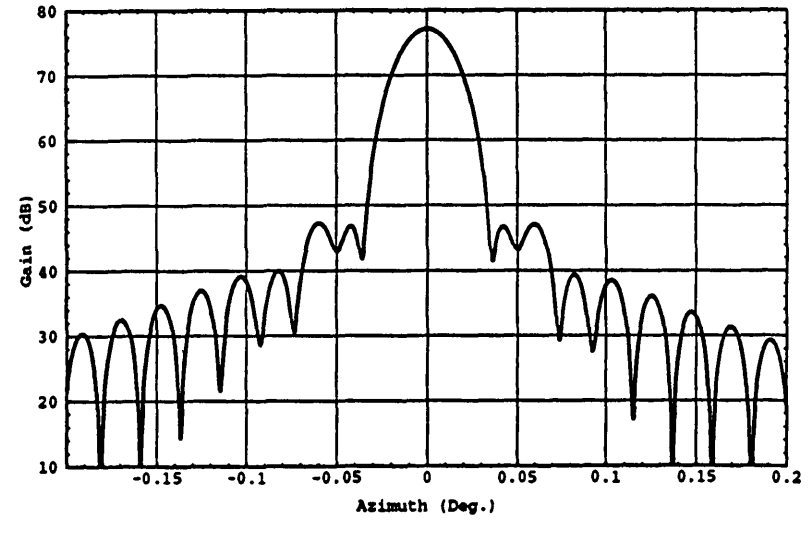

(b) Asymmetric plane

Fig. 12. Far-field pattern at 8.00 GHz at zenith after correction.

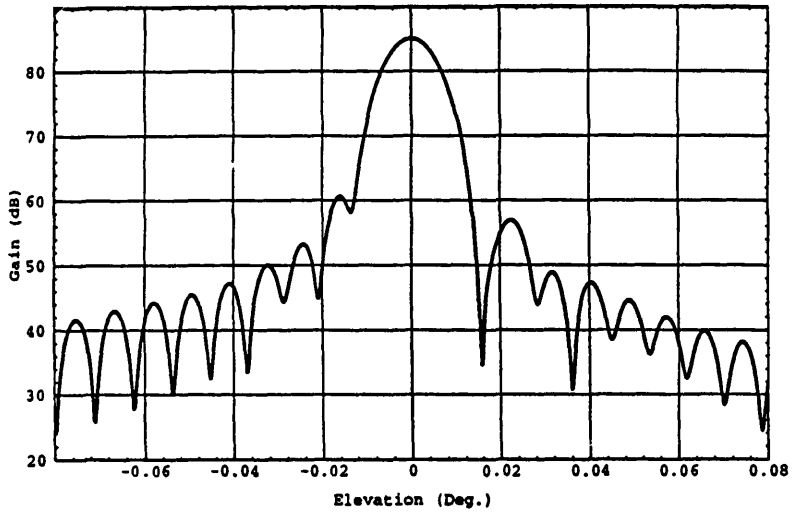

(a) Symmetric plane

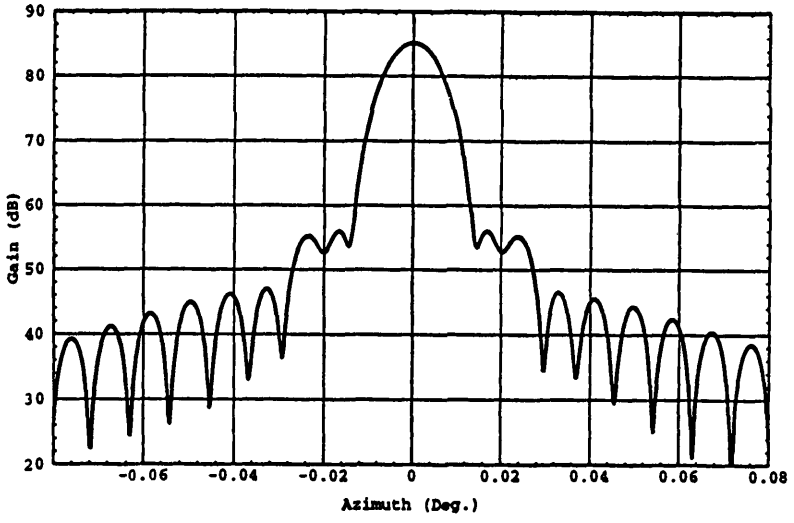

(b) Asymmetric plane

Fig. 13. Far-field pattern at 20.00 GHz at zenith after correction.

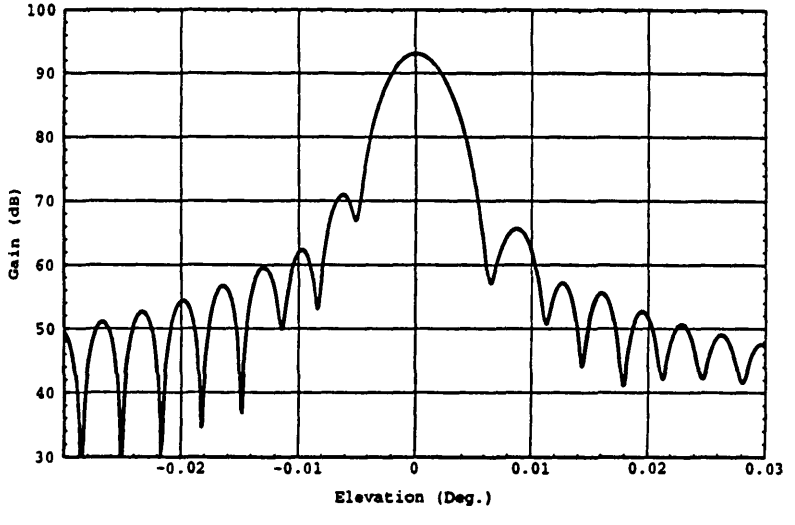

(a) Symmetric plane

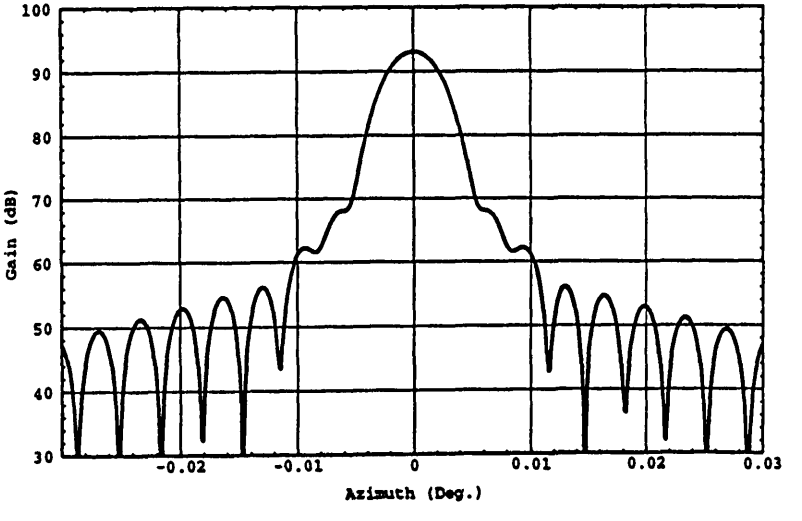

(b) Asymmetric plane

Fig. 14. Far-field pattern at 50.00 GHz at zenith after correction.